



Thermodynamic characterization of boltwoodite and uranophane: Enthalpy of formation and aqueous solubility

Tatiana Y. Shvareva^a, Lena Mazeina^{a,1}, Drew Gorman-Lewis^{b,2}, Peter C. Burns^b,
Jennifer E.S. Szymanowski^b, Jeremy B. Fein^b, Alexandra Navrotsky^{a,*}

^a Peter A. Rock Thermochemistry Laboratory, University of California, Davis, One Shields Avenue, Davis, CA 95616, United States

^b University of Notre Dame, Department of Civil Engineering and Geological Sciences, 156 Fitzpatrick Hall,
Notre Dame, IN 46556, United States

Received 9 December 2010; accepted in revised form 21 June 2011; available online 5 July 2011

Abstract

Boltwoodite and uranophane are uranyl silicates common in oxidized zones of uranium ore deposits. An understanding of processes that impact uranium transport in the environment, especially pertaining to the distribution of uranium between solid phases and aqueous solutions, ultimately requires determination of thermodynamic parameters for such crystalline materials. We measured formation enthalpies of synthetic boltwoodites, $K(\text{UO}_2)(\text{HSiO}_4) \cdot \text{H}_2\text{O}$ and $\text{Na}(\text{UO}_2)(\text{HSiO}_4) \cdot \text{H}_2\text{O}$, and uranophane, $\text{Ca}(\text{UO}_2)_2(\text{HSiO}_4)_2 \cdot 5\text{H}_2\text{O}$, by high temperature oxide melt solution calorimetry. We also studied the aqueous solubility of these phases from both saturated and undersaturated conditions at a variety of pH. The combined data permit the determination of standard enthalpies, entropies and Gibbs free energies of formation for each phase and analysis of its potential geological impact from a thermodynamic point of view.

© 2011 Elsevier Ltd. All rights reserved.

1. INTRODUCTION

Uranyl minerals, which contain U^{6+} , are important constituents in the oxidized zones of uranium ore deposits. An understanding of the stabilities and properties of these materials is essential to model the distribution of uranium in near-surface conditions, either in uranium deposits or sites that have been contaminated by uranium. Of the uranyl minerals, uranyl silicates such as uranophane and boltwoodite are among the most common. They form as alteration products of spent nuclear fuel and other radioac-

tive materials under moist oxidizing conditions (Finch and Ewing, 1992; Wronkiewicz et al., 1992, 1996), and can form in the vadose zone following release of uranium into the subsurface (Catalano et al., 2004). Although processes such as adsorption of uranium onto mineral surfaces and bacteria, bacterial-mediated reduction of U(VI) (Arnold et al., 2010), co-precipitation of uranium with other minerals, and attachment of uranium to colloids may also affect the environmental mobility of uranium (Barger et al., 2008; Langmuir, 1978; Nitsche, 1997), the thermodynamic stability of uranyl minerals is responsible for redistribution of uranium between solid and aqueous phases under geologic conditions. Thus, the creation of a comprehensive internally-consistent thermodynamic database for all environmentally-relevant uranyl phases is essential for assessment and modeling of uranium transport in natural and anthropogenic settings.

Enthalpies of formation measured by high temperature oxide melt solution calorimetry have been reported for several uranyl oxide hydrates: metaschoepite $\text{UO}_3(\text{H}_2\text{O})_2$,

* Corresponding author. Tel.: +530 752 3292; fax: +530 752 9307.

E-mail address: anavrotsky@ucdavis.edu (A. Navrotsky).

¹ Present address: Technology Assessment and Transfer, Millersville, MD 21108, United States.

² Present address: University of Washington, Department of Earth and Space Sciences, 070 Johnson Hall, Seattle, WA 98195, United States.

β - $\text{UO}_2(\text{OH})_2$, CaUO_4 , becquerelite $\text{Ca}[(\text{UO}_2)_3\text{O}_2(\text{OH})_3]_2 \cdot 8\text{H}_2\text{O}$, $\text{Ca}(\text{UO}_2)_4\text{O}_3(\text{OH})_4 \cdot 2\text{H}_2\text{O}$, clarkeite $\text{Na}(\text{UO}_2)\text{O}(\text{OH})$, and Na-compreignacite $\text{Na}_2[(\text{UO}_2)_3\text{O}_2(\text{OH})_3]_2 \cdot 7\text{H}_2\text{O}$, and curite $\text{Pb}_2(\text{UO}_2)_8\text{O}_8(\text{OH})_6 \cdot 2\text{H}_2\text{O}$ (Kubatko et al., 2006); and for several uranyl carbonates: rutherfordine UO_2CO_3 , andersonite $\text{Na}_2\text{Ca}[(\text{UO}_2)(\text{CO}_3)_3] \cdot 5\text{H}_2\text{O}$, and grimselite $\text{K}_3\text{NaUO}_2(\text{CO}_3)_3 \cdot \text{H}_2\text{O}$ (Kubatko et al., 2005). Enthalpies of formation, together with Gibbs free energies of formation of these phases derived from solubility measurements, can be used to calculate entropies of formation as well, and this approach has been applied to a range of uranyl oxide hydrate phases (Gorman-Lewis et al., 2008a), uranyl phosphate phases (Gorman-Lewis et al., 2009), and to the uranyl silicate soddyite (Gorman-Lewis et al., 2007).

Uranyl silicates, including soddyite, uranophane $\text{Ca}(\text{UO}_2)_2(\text{HSiO}_4)_2 \cdot 5\text{H}_2\text{O}$, and boltwoodite $(\text{Na},\text{K})(\text{UO}_2)(\text{HSiO}_4) \cdot \text{H}_2\text{O}$, are important minerals associated with alteration of spent nuclear fuel under moist oxidizing conditions. Studies of natural analogues to spent fuel alteration have demonstrated the importance of the uranyl silicates (Pearcy et al., 1994). Studies of UO_2 conducted under oxidizing conditions using Si-rich water revealed the formation of uranyl silicate minerals (Wronkiewicz et al. 1992, 1996), as did similar experiments using radioactive used nuclear fuel (Finch and Hawthorne, 1998). Deditius et al. (2007) showed that Na- and K-boltwoodite are the products of the oxidation of coffinite $\text{USiO}_4 \cdot n\text{H}_2\text{O}$. Recently, boltwoodite and uranophane were found as uranium-bearing precipitates in the vadose zone of the Hanford Site, where uranium was released during weapons-related activities (Catalano et al., 2004; Um et al., 2009).

In this study we extend the existing database and report enthalpies, solubilities, Gibbs free energies of formation, entropies of formation, and standard entropies for Na-boltwoodite $\text{Na}(\text{UO}_2)(\text{HSiO}_4) \cdot \text{H}_2\text{O}$, boltwoodite $\text{K}(\text{UO}_2)(\text{HSiO}_4) \cdot \text{H}_2\text{O}$, and uranophane $\text{Ca}(\text{UO}_2)_2(\text{HSiO}_4)_2 \cdot 5\text{H}_2\text{O}$. With these parameters, we evaluate the stabilities of the phases relative to other uranyl mineral species under environmentally-relevant conditions.

2. EXPERIMENTAL METHODS

2.1. Syntheses of solid phases

ACS grade reagents and 18 M Ω H_2O were used in all syntheses. Teflon lined Parr reaction vessels were used for the hydrothermal treatments of the starting material. Teflon liners in the Parr pressure vessels were conditioned by at least eight heating cycles with H_2O prior to use to minimize release of impurities into the synthesis solutions. Consistent starting materials are essential for reliable syntheses of uranyl compounds; therefore, amorphous UO_3 and $\text{UO}_2(\text{CH}_3\text{COO})_2 \cdot 2\text{H}_2\text{O}$ were prepared for each synthesis using the following procedures. UO_3 was prepared by dissolving commercially available UO_3 in ~ 6 M HNO_3 and heating the solution to dryness until all gases had evolved and the solid had a uniform orange color. $\text{UO}_2(\text{CH}_3\text{COO})_2 \cdot 2\text{H}_2\text{O}$ was prepared by gently heating (just below

boiling) ~ 0.5 g of the freshly prepared UO_3 with ~ 600 cm³ glacial acetic acid until dryness.

Na-boltwoodite was synthesized by combining 0.175 g of purified uranyl acetate, 0.5 mL of 1 M $\text{NaSiO}_3 \cdot 5\text{H}_2\text{O}$, and 4.75 mL of H_2O in a Teflon lined Parr reaction vessel. The solution pH was adjusted to ca. 11 using 6 M NaOH, and was heated at 150 °C for 7 days. The heat treatment produced a gelatinous material. After rinsing the gel with boiling water and allowing it to air dry, the resulting powder was soaked in 15 mL of 6 M NaOH for 10 min. Filtering the mineral/NaOH solution through a 10 μm PTFE filter under vacuum and rinsing it with three 25 mL aliquots of room temperature H_2O produced a flaky light yellow powder.

Boltwoodite was synthesized by combining 0.160 g of freshly prepared uranyl acetate, 0.024 g of SiO_2 as powder, 0.5 mL of 6 M KOH, and 4.5 mL of H_2O in a Teflon lined Parr reaction vessel. The solution was heated at 180 °C for 7 days. Subsequent processing was identical to the Na-boltwoodite synthesis with the exception that 6 M KOH was used for soaking instead of NaOH. Similar to the Na-boltwoodite procedure, this synthesis yielded a flaky light yellow powder.

Uranophane was synthesized by combining 0.200 g of $\text{NaSiO}_3 \cdot 9\text{H}_2\text{O}$, 0.080 g of $\text{Ca}(\text{CH}_3\text{COO})_2 \cdot \text{H}_2\text{O}$, 0.160 g of purified uranyl acetate, and 4.0 mL of H_2O in a Teflon lined Parr reaction vessel. The solution was heated at 100 °C for 72 h and the resulting yellow powder was rinsed four times using boiling H_2O .

2.2. Characterization

X-ray powder diffraction (XRD) patterns were collected for each synthesis product by grinding ~ 5 mg of sample into a fine powder with water for uranophane and ethanol for boltwoodite and Na-boltwoodite and depositing the paste onto a zero-background quartz slide. Diffraction patterns were collected using a Bruker D8 Discovery diffractometer equipped with $\text{CuK}\alpha$ radiation and a solid-state detector. FT-IR analyses were performed using an IlluminatIR FT-IR microspectrometer with a diamond total attenuated reflectance (ATR) objective in an open atmosphere. Background spectra were taken prior to each measurement, which were done over a frequency range of 400–4000 cm⁻¹ using ~ 5 –10 mg of powder placed on a glass slide. IR spectra were in good agreement with previously published spectra (Cejka, 1999). XRD patterns are reported in the Supplemental Materials.

Chemical analyses were performed for solutions created by dissolving ~ 5 –10 mg of powder in ~ 50 mL of 2 M HCl. The solutions were analyzed for total aqueous uranium, sodium, potassium, and silicon using inductively coupled plasma optical emission spectrometry (ICP-OES) with an analytical uncertainty of 3.5%. Water content was determined from weight loss using a Netsch 449 TGA/DSC instrument. Two specimens of each phase were heated to 800 °C at 10 °C/min under flowing argon at 50 mL/min.

After characterization, the products of several synthesis reactions were combined in a single reaction vessel, and

homogenized by mixing with a spatula, and used in the solubility and calorimetric experiments described below.

2.3. Solubility experiments

All solubility measurements were conducted as batch experiments using Teflon reaction vessels at 22 °C. An Orion combination pH electrode calibrated daily with four NIST standards (pH 2, 4, 7, and 10) was used for pH measurements. The ionic strength of the buffers was not perfectly matched to the ionic strength of the experiments; however, the additional error associated with pH measurements as a result of the difference in ionic strength and liquid-junction error is likely much smaller than experimental error that dominates the stated uncertainties for the calculated thermodynamic parameters (Illingworth, 1981). Boltwoodite and Na-boltwoodite experiments were done in either 50 mM KNO_3 or NaNO_3 to buffer ionic strength. The experiments using uranophane were not buffered for ionic strength. Boltwoodite and Na-boltwoodite undersaturated experiments were conducted by adding ~ 350 mg of the synthesized phase of interest to ~ 120 cm³ of electrolyte; the supersaturated experiments involved adding ~ 350 mg of the mineral phase to electrolyte solutions that already contained dissolved U and Si from additions of $\text{UO}_2(\text{NO}_3)_2$ and an aqueous Si ICP standard.

Initial uranophane solubility experiments resulted in the formation of amorphous silica as the uranophane – aqueous solution reaction reached a steady-state. Consequently, silica gel was added to subsequent experiments in order to attain steady-state faster and to buffer aqueous silica concentrations. The solid phase composition of the experimental systems contained ~ 400 mg of uranophane and ~ 300 mg of silica gel and the solution phase contained U and Ca in the same molal ratio as in uranophane. The concentrations of U and Ca were varied to achieve supersaturated and undersaturated starting conditions with respect to U and Ca; Si was added to the solution to achieve an aqueous concentration close to the amorphous silica solubility limit.

Experimental systems were all prepared open to the atmosphere and then sealed during agitation. The headspace of the systems was refreshed by opening vials to the atmosphere periodically during sampling and pH monitoring. For all experimental systems, pH was adjusted to a target pH (see Fig. 2–4 for target pH values) using minute quantities of concentrated HNO_3 and/or NaOH or KOH . The pH was monitored daily and adjusted as needed throughout each experiment. For each experiment, the pH descriptor is the average of the pH values for the solubility plateau data points; however, the actual pH measurement for each data point was used in the subsequent thermodynamic calculations. Reaction vessels were sealed and agitated slowly end over end at room temperature. Aliquots of the experimental solution were extracted at various times, filtered through 0.1 μm Millipore Millex filters, and diluted and acidified for ICP-OES analysis to determine dissolved concentrations of U, Si, Na, and K. Control experiments verified that loss of uranium through adsorption to the filter membrane and reaction vessel was negligible. In

order to verify the composition of the mineral residue at the end of each experiment, ~ 10 mg of residue was collected for XRD and FT-IR analysis.

2.4. Calorimetry

Molten oxide drop solution calorimetry was performed using a custom-built Tian-Calvet high temperature micro-calorimeter (Navrotsky, 1977, 1997). The methodology of measuring drop solution enthalpies for uranyl-based minerals in sodium molybdate at 700 °C is well established (Gorman-Lewis et al., 2007; Kubatko et al., 2006, 2005). Drop solution enthalpies, ΔH_{ds} , were used to calculate enthalpies of formation using the calorimetric cycles depicted in Table 1. The final state of SiO_2 in these experiments, as determined earlier (Gorman-Lewis et al., 2007), is cristobalite. To accelerate precipitation of SiO_2 as cristobalite and to obtain consistent values of ΔH_{ds} , 50 mg of cristobalite was added to the solvent prior to dropping the samples.

3. RESULTS AND DISCUSSION

3.1. Characterization

All observed powder diffraction patterns of Na-boltwoodite, boltwoodite and uranophane exhibit sharp profiles and no extraneous peaks, confirming the synthesized mineral as the only crystalline phase (Supplemental Materials Figures S1–S3). Thermogravimetry/differential scanning calorimetry (TG/DSC) data for all materials confirm the presence of structural water in the samples (Table 2). Thermogravimetric curves for Na- and K-boltwoodite have two pronounced weight loss steps. The first step, in the temperature range 80–525 °C for Na-boltwoodite and 75–590 °C for K-boltwoodite, is profound and can be attributed to the elimination of water from the interlayer space. Water content calculated from these data corresponds to the presence of 1.25 and 0.97 moles of water molecules in Na-boltwoodite and K-boltwoodite, respectively. These results are in agreement with structural analysis (Burns, 1998). The

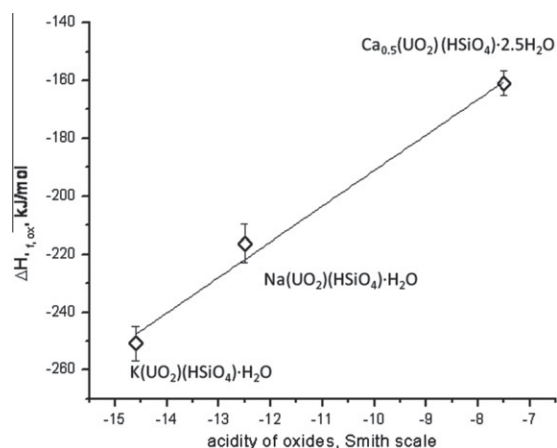


Fig. 1. Enthalpy of formation of uranophane, boltwoodite and Na-boltwoodite from oxides as a function of acidity of the oxides on the Smith scale (Smith, 1987).

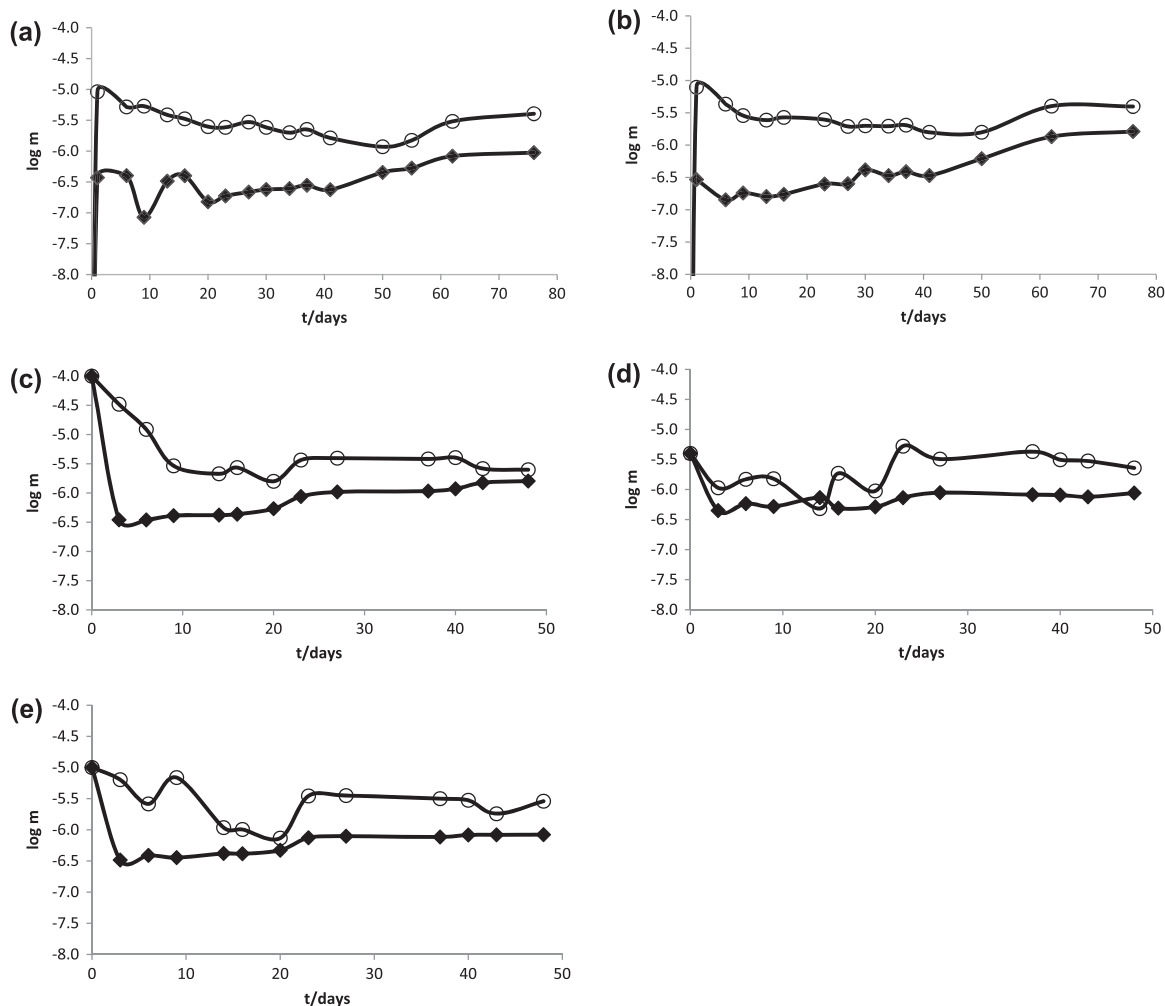


Fig. 2. Experimental measurements of the solubility of boltwoodite in terms of dissolved U (closed diamonds) and Si (open circles) as a function of time from undersaturation with respect to U for experiments at pH 7.6 (a) and pH 8.0 (b) and from supersaturation with respect to U for experiments at pH 8.5 (c), pH 8.0 (d), and pH 7.4 (e).

second more gradual weight loss up to 750 °C for both materials may be caused by the continuous loss of OH⁻ groups of silicate tetrahedra that also extend into the interlayer region. The number of moles of water calculated from this second step corresponds to the proton occupancy near the terminal oxygen of silicate tetrahedra. Table 2 shows the measured proton content.

The TG curve for uranophane exhibits three plateaus and agrees well with results reported in the literature (Urbanec et al., 1985). The first two steps are assigned in the literature to the loss of interlayer water. The third step is much less pronounced and has not been assigned to any particular water arrangement in previous studies. By analogy to boltwoodite, we attribute this third step to structural hydroxyl dehydration.

In order to determine the correct stoichiometry for each phase, the measured chemical composition was combined with the thermogravimetric data (Table 2), resulting in the compositions of Na_{0.93}(UO₂)(H_{0.85}SiO₄)_{0.93}·1.29H₂O, K_{0.75}(UO₂)(H_{0.80}SiO₄)_{0.86}·0.97H₂O, and Ca_{1.09}(UO₂)₂-

(H_{0.51}SiO₄)_{1.77}·5.55H₂O for Na-boltwoodite, boltwoodite and uranophane, respectively. An extra significant digit in the chemical composition is retained to preserve charge balance. The formulas show good correlation between partial occupancy of the protons determined by the TG analysis and the H-content calculated from charge balance (Table 2). These formulas were used in the calculations of formation enthalpy according to the thermodynamic cycles (Table 1).

3.2. Enthalpies of formation

Drop solution enthalpies measured in sodium molybdate solvent at 702 °C are 276.5 ± 5.1, 266.3 ± 4.6 and 731.9 ± 8.0 kJ/mol for Na-, K-boltwoodite and uranophane, respectively. These data result in negative formation enthalpies from constituent oxides: -215.8 ± 6.0 kJ/mol for Na-boltwoodite Na_{0.93}(UO₂)(H_{0.85}SiO₄)_{0.93}·1.29H₂O, -251.2 ± 5.9 kJ/mol for boltwoodite K_{0.75}(UO₂)(H_{0.80}SiO₄)_{0.86}·0.97H₂O, and -322.1 ± 10.7 kJ/mol for uranophane

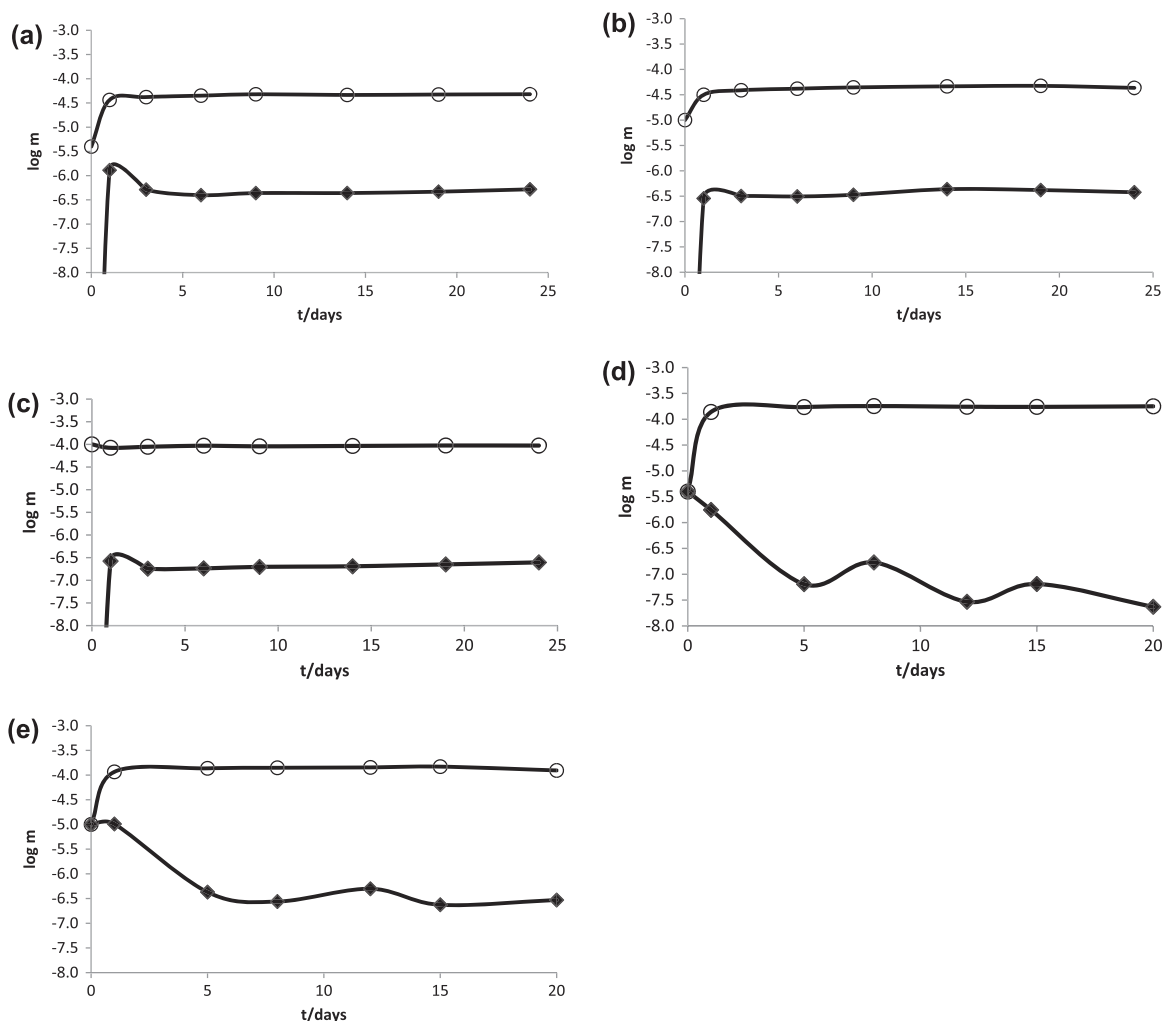


Fig. 3. Experimental measurements of the solubility of Na-boltwoodite in terms of dissolved U (closed diamonds) and Si (open circles) as a function of time from undersaturation with respect to U for experiments at pH 7.4 (a), pH 7.7 (b), and pH 8.2 (c) and from supersaturation with respect to U for experiments at, pH 7.7 (d), and pH 8.0 (e).

$\text{Ca}_{1.09}(\text{UO}_2)_2(\text{H}_{0.51}\text{SiO}_4)_{1.77} \cdot 5.55\text{H}_2\text{O}$, indicating significant stability of these phases relative to UO_3 , quartz and H_2O (Table 3).

The slight deviations in the composition of each phase from the ideal stoichiometry result in complex chemical formulas and make further data evaluation difficult. However, the drop solution enthalpy is a unique characteristic measured for each material of a specific composition, and, therefore, it cannot be readily extrapolated to other compositions. In the thermodynamic cycles shown in Table 1, we use the corresponding amount of oxides and/or elements to balance non-ideal stoichiometry and to calculate the correct formation enthalpies for each phase studied here. It has been reported in previous research (Ushakov et al., 2002) that if a secondary phase, site vacancies or interstitial formation do not occur within a sample, formation enthalpies from the oxides of slightly non-stoichiometric phases do not deviate from the values for stoichiometric compounds by more than the uncertainty of the calorimetric measurements. Thus, for the uranyl silicate hydroxides in this study,

we base all of the following thermodynamic and solubility calculations on the stoichiometric formula of each material assuming that the enthalpy of formation from oxides is the same as that measured for the slightly non-stoichiometric materials.

In Table 3 we report measured enthalpies, entropies and Gibbs free energies of formation from oxides and from elements, calculated from high temperature oxide calorimetry and solubility measurements, as well as previously predicted values (Clark et al., 1998), for soddyite, boltwoodite, and uranophane. All values are normalized to one uranyl unit per formula for easier comparison. The least exothermic formation enthalpy from oxides among uranyl silicates, -117.8 ± 4.3 kJ/mol, is observed for soddyite $(\text{UO}_2)_2(\text{SiO}_4) \cdot 2\text{H}_2\text{O}$ (or -58.9 ± 2.2 kJ/mol per $(\text{UO}_2)(\text{SiO}_4)_{0.5} \cdot \text{H}_2\text{O}$ unit) (Gorman-Lewis et al., 2007). Soddyite, the compositionally simplest uranyl silicate, is composed of uranyl silicate chains formed by edge-sharing uranyl pentagonal bipyramids and silicate tetrahedra, joined together through uranyl pentagonal bipyramids into a three-dimensional

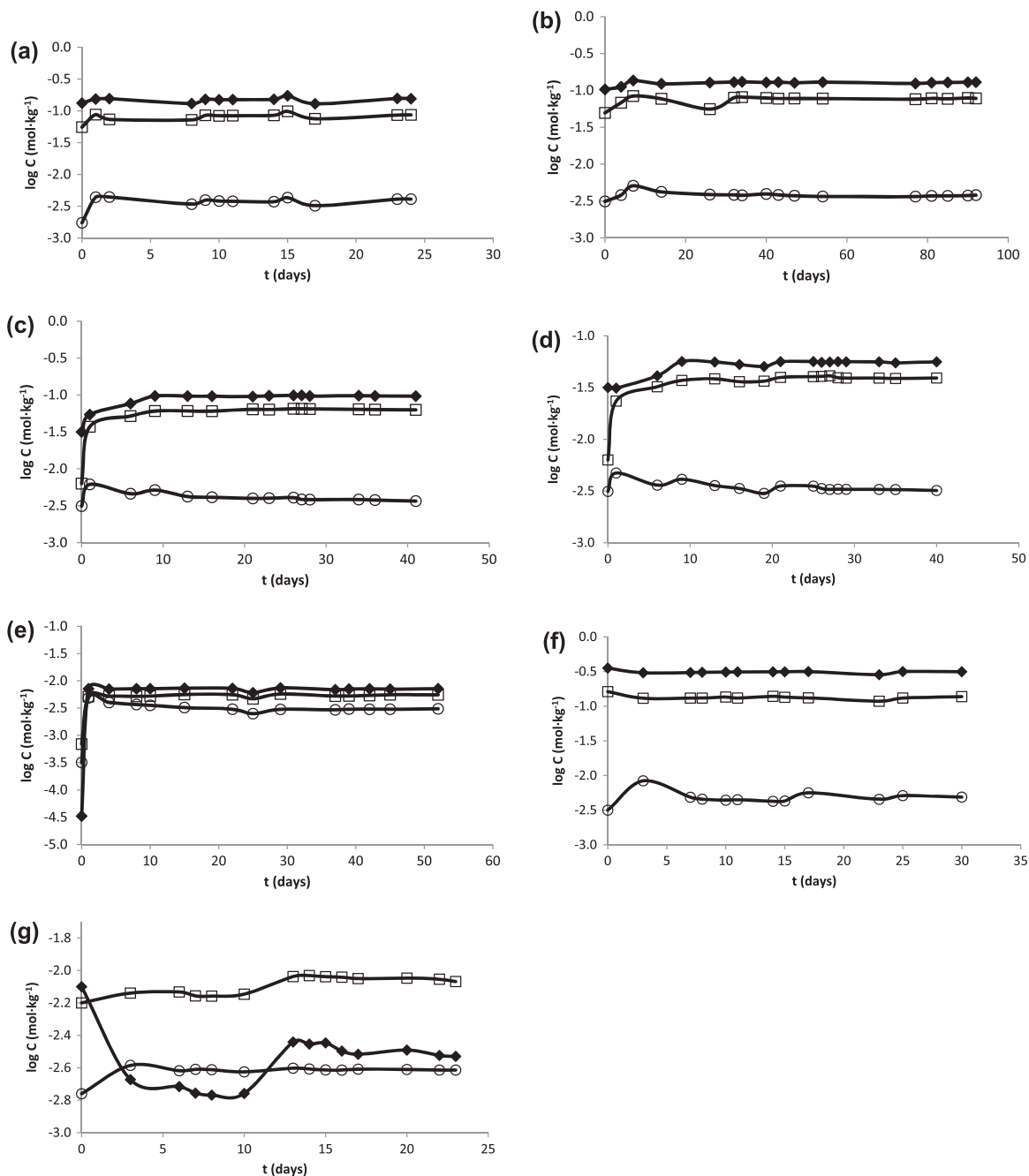


Fig. 4. Experimental measurements of the solubility of uranophane in terms of dissolved U (closed diamonds), Si (open circles), and Ca (open squares) as a function of time from undersaturation with respect to U for experiments at pH 3.2 (a), pH 3.3 (b), pH 3.4 (c), pH 3.5 (d), and pH 3.9 (e), and from supersaturation with respect to U for experiments at pH 3.0 (f) and pH 4.0 (g).

framework structure (Demartin et al., 1992; Burns, 2005). The sheets in the structures of Na-boltwoodite, boltwoodite, and uranophane are identical and consist of chains with the same topology as in soddyite. These chains are arranged in two-dimensional uranyl silicate layers with K⁺, Na⁺, Ca²⁺ and H₂O located in interlayer spaces (Burns, 2005). In addition to Lewis interactions between UO₃ and SiO₂ as in soddyite, acid-base interactions between CaO, Na₂O, and K₂O, respectively, and SiO₂ contribute to the enthalpies of formation, making them more exothermic as

the oxides become more basic (Table 3). As shown, for example, for the case of ACoPO₄ and AZnPO₄ (where A = Na⁺, K⁺, Rb⁺ and NH₄⁺) (Le and Navrotsky, 2007, 2008), the enthalpy of formation from constituent oxides changes linearly with the acidity of the alkali oxides. The most negative formation enthalpies correspond to the least acidic cationic oxide K₂O. Analogously, we plot enthalpies of formation of the uranyl silicates Na-boltwoodite, boltwoodite and uranophane from oxides as a function of cation acidity using the Smith scale (Smith, 1987) and observe

Table 1
Thermodynamic cycles for enthalpy calculations of samples from oxides and elements.

<i>Na-boltwoodite</i> $Na_{0.93}(UO_2)(H_{0.85}SiO_4)_{0.93} \cdot 1.25H_2O$	
$Na_{0.93}(UO_2)(H_{0.85}SiO_4)_{0.93} \cdot 1.25H_2O$ xl, 25 °C = UO_3 sln, 702 °C + $0.93SiO_2$ sln, cr, 702 °C + $0.47Na_2O$ sln, 702 °C + (1.25+0.40) H_2O g, 702 °C	$\Delta H1 = \Delta H_{ds} = 276.5 \pm 5.1$ kJ/mol (10)
UO_3 xl, 25 °C = UO_3 sln, 702 °C	$\Delta H2 = \Delta H_{ds}(UO_3) = 9.5 \pm 1.5$ kJ/mol Helean et al., (2002)
SiO_2 xl, cr, 25 °C = SiO_2 sln, 702 °C	$\Delta H3 = \Delta H_{ds}(SiO_2) = 40.6 \pm 0.6$ kJ/mol Gorman-Lewis et al. (2007)
Na_2O xl, 25 °C = Na_2O sln, 702 °C	$\Delta H4 = \Delta H_{ds}(Na_2O) = -215.8 \pm 4.4$ kJ/mol Tessier and Navrotsky (2000)
H_2O l, 25 °C = H_2O g, 702 °C	$\Delta H5 = \Delta H_{ds}(H_2O) = 69.0 \pm 1.0$ kJ/mol Robie and Hemingway (1995)
UO_3 xl, 25 °C + $0.93SiO_2$ xl, 25 °C + $0.47Na_2O$ xl, 25 °C + (1.25+0.40) H_2O l, 25 °C =	$\Delta H6 = \Delta H_{f, ox} = -\Delta H1 + \Delta H2 + 0.93\Delta H3 + 0.47\Delta H4 + 1.65\Delta H5 = -215.8 \pm 6.0$ kJ/mol
<i>Na-boltwoodite</i> $Na_{0.93}(UO_2)(H_{0.85}SiO_4)_{0.93} \cdot 1.25H_2O$ xl, 25 °C	$\Delta H7 = \Delta H_f(UO_3) = -1223.8 \pm 0.8$ kJ/mol
U xl, 25 °C + $3/2 O_2$ g, 25 °C = UO_3 xl, 25 °C	$\Delta H8 = \Delta H_f(SiO_2) = -908.4 \pm 2.1$ kJ/mol Robie and Hemingway (1995)
Si xl, 25 °C + O_2 g, 25 °C = SiO_2 xl, cr, 25 °C	$\Delta H9 = \Delta H_f(Na_2O) = -414.8 \pm 0.3$ kJ/mol Robie and Hemingway (1995)
$2Na$ xl, 25 °C + $1/2 O_2$ g, 25 °C = Na_2O xl, 25 °C	$\Delta H10 = \Delta H_f(H_2O) = -285.8 \pm 0.1$ kJ/mol Robie and Hemingway (1995)
H_2 g, 25 °C + $1/2 O_2$ g, 25 °C = H_2O l, 25 °C	$\Delta H11 = \Delta H_{f, el} = \Delta H6 + \Delta H7 + 0.93\Delta H8 + 0.47\Delta H9 + 1.665\Delta H10 = -2948.8 \pm 6.6$ kJ/mol
U xl, 25 °C + $0.93Si$ xl, 25 °C + $0.93Na$ xl, 25 °C + $1.65H_2$ g, 25 °C + $3.42O_2$ g, 25 °C = $Na_{0.93}(UO_2)(H_{0.85}SiO_4)_{0.93} \cdot 1.25H_2O$ xl, 25 °C	$\Delta H12 = \Delta H_{ds} = 266.3 \pm 4.6$ kJ/mol (10)
<i>K-boltwoodite</i> $K_{0.75}(UO_2)(H_{0.80}SiO_4)_{0.86} \cdot 0.97H_2O$	$\Delta H2 = \Delta H_{ds}(UO_3) = 9.5 \pm 1.5$ kJ/mol Helean et al., (2002)
$K_{0.75}(UO_2)(H_{0.80}SiO_4)_{0.86} \cdot 0.97H_2O$ xl, 25 °C = UO_3 sln, 702 °C + $0.86SiO_2$ sln, cr, 702 °C + $0.38K_2O$ sln, 702 °C + (0.97 + 0.34) H_2O g, 702 °C	$\Delta H3 = \Delta H_{ds}(SiO_2) = 40.6 \pm 0.6$ kJ/mol Gorman-Lewis et al. (2007)
UO_3 xl, 25 °C = UO_3 sln, 702 °C	$\Delta H13 = \Delta H_{ds}(K_2O) = -319.2 \pm 4.6$ kJ/mol Ushakov et al. (2004)
SiO_2 xl, cr, 25 °C = SiO_2 sln, 702 °C	$\Delta H5 = \Delta H_{ds}(H_2O) = 69.0 \pm 1.0$ kJ/mol Robie and Hemingway (1995)
K_2O xl, 25 °C = K_2O sln, 702 °C	$\Delta H14 = \Delta H_{f, ox} = -\Delta H12 + \Delta H2 + 0.86\Delta H3 + 0.38\Delta H13 + 1.31\Delta H5 = -251.2 \pm 5.9$ kJ/mol
H_2O l, 25 °C = H_2O g, 702 °C	$\Delta H7 = \Delta H_f(UO_3) = -1223.8 \pm 0.8$ kJ/mol
UO_3 xl, 25 °C + $0.86SiO_2$ xl, 25 °C + $0.38K_2O$ xl, 25 °C + (0.97+0.34) H_2O l, 25 °C = $K_{0.75}(UO_2)(H_{0.80}SiO_4)_{0.86} \cdot 0.97H_2O$ xl, 25 °C	$\Delta H8 = \Delta H_f(SiO_2) = -908.4 \pm 2.1$ kJ/mol Robie and Hemingway (1995)
U xl, 25 °C + $3/2 O_2$ g, 25 °C = UO_3 xl, 25 °C	$\Delta H15 = \Delta H_{f, el}(K_2O) = -363.2 \pm 2.1$ kJ/mol Robie and Hemingway (1995)
Si xl, 25 °C + O_2 g, 25 °C = SiO_2 xl, cr, 25 °C	$\Delta H10 = \Delta H_f(H_2O) = -285.8 \pm 0.1$ kJ/mol Robie and Hemingway (1995)
$2K$ xl, 25 °C + $1/2 O_2$ g, 25 °C = K_2O xl, 25 °C	$\Delta H16 = \Delta H_{f, el} = -\Delta H13 + \Delta H7 + 0.86\Delta H8 + 0.38\Delta H14 + 1.31\Delta H10 = -2766.8 \pm 6.5$ kJ/mol
H_2 g, 25 °C + $1/2 O_2$ g, 25 °C = H_2O l, 25 °C	$\Delta H17 = \Delta H_{ds} = 731.9 \pm 8.0$ kJ/mol (10)
U xl, 25 °C + $0.86Si$ xl, 25 °C + $0.38K$ xl, 25 °C + $1.31 H_2$ g, 25 °C + $3.21 O_2$ g, 25 °C = $K_{0.75}(UO_2)(H_{0.80}SiO_4)_{0.86} \cdot 0.97H_2O$ xl, 25 °C	$\Delta H2 = \Delta H_{ds}(UO_3) = 9.5 \pm 1.5$ kJ/mol Helean et al., (2002)
<i>Uranophane</i> $Ca_{1.09}(UO_2)_2(H_{0.51}SiO_4)_{1.77} \cdot 5.60H_2O$	$\Delta H3 = \Delta H_{ds}(SiO_2) = 40.6 \pm 0.6$ kJ/mol Gorman-Lewis et al. (2007)
$Ca_{1.09}(UO_2)_2(H_{0.51}SiO_4)_{1.77} \cdot 5.60H_2O$ xl, 25 °C = $2UO_3$ sln, 702 °C + $1.77 SiO_2$ sln, cr, 702 °C + $1.09CaO$ sln, 702 °C + (5.60 + 0.45) H_2O g, 702 °C	$\Delta H18 = \Delta H_{ds}(CaO) = -90.5 \pm 1.8$ kJ/mol Kubatko et al. (2005)
UO_3 xl, 25 °C = UO_3 sln, 702 °C	$\Delta H5 = \Delta H_{ds}(H_2O) = 69.0 \pm 1.0$ kJ/mol Robie and Hemingway (1995)
SiO_2 xl, cr, 25 °C = SiO_2 sln, 702 °C	$\Delta H19 = \Delta H_{f, ox} = -\Delta H16 + 2\Delta H2 + 1.77$
CaO xl, 25 °C = CaO sln, 702 °C	$\Delta H3 + 1.09\Delta H17 + 6.05\Delta H5 = -322.2 \pm 10.7$ kJ/mol
H_2O l, 25 °C = H_2O g, 702 °C	$\Delta H7 = \Delta H_f(UO_3) = -1223.8 \pm 0.8$ kJ/mol
$2UO_3$ xl, 25 °C + $1.77SiO_2$ xl, 25 °C + $1.09 CaO$ xl, 25 °C + (5.60+0.45) H_2O l, 25 °C = $Ca_{1.09}(UO_2)_2(H_{0.51}SiO_4)_{1.77} \cdot 5.60H_2O$ xl, 25 °C	$\Delta H8 = \Delta H_f(SiO_2) = -908.4 \pm 2.1$ kJ/mol Robie and Hemingway (1995)
U xl, 25 °C + $3/2 O_2$ g, 25 °C = UO_3 xl, 25 °C	$\Delta H20 = \Delta H_f(CaO) = -635.1 \pm 0.3$ kJ/mol Robie and Hemingway (1995)
Si xl, 25 °C + O_2 g, 25 °C = SiO_2 xl, cr, 25 °C	$\Delta H10 = \Delta H_f(H_2O) = -285.8 \pm 0.1$ kJ/mol Robie and Hemingway (1995)
Ca xl, 25 °C + $1/2 O_2$ g, 25 °C = CaO xl, 25 °C	$\Delta H21 = \Delta H_{f, el} = -\Delta H12 + \Delta H13 + 1.77\Delta H14 + 1.09\Delta H16 + 6.05\Delta H15 = -6799.0 \pm 11.5$ kJ/mol
H_2 g, 25 °C + $1/2 O_2$ g, 25 °C = H_2O l, 25 °C	
U xl, 25 °C + $1.77Si$ xl, 25 °C + $1.09Ca$ xl, 25 °C + $6.05H_2$ g, 25 °C + $14.68O_2$ g, 25 °C = $Ca_{1.09}(UO_2)_2(H_{0.51}SiO_4)_{1.77} \cdot 5.60H_2O$ xl, 25 °C	

Number in parentheses indicates the number of drops

xl – crystalline phase.

sln – dissolved phase.

g – gas phase.

cr - crystalalite.

ΔH_{ds} – enthalpy of drop solution.

$\Delta H_{f, ox}$ – enthalpy of formation from oxides.

$\Delta H_{f, el}$ – enthalpy of formation from elements.

a similar linear relationship, with the strongest contribution from the most basic oxide K_2O (Fig. 1). The strong linear correlation of formation enthalpies with acidity and ionic potential of cations provides additional confirmation of our assumption of the absence of any specific interaction within the uranyl silicate structures. It is interesting that the linear trend is observed even with different amounts of structural water.

3.3. Solubility experiments

Undersaturated experiments concerning the boltwoodite – aqueous solution reaction required at least 62 days to reach steady-state conditions (Fig. 2a and b), while supersaturated experiments reached steady-state conditions within 23 days (Fig. 2c and d). All experiments exhibited similar extents of non-stoichiometric dissolution, with Si in excess of U in solution by less than an order of magnitude. X-ray powder diffraction (XRD) analysis of mineral residues indicated that boltwoodite was the only crystalline phase detected. Precipitation of an amorphous phase could produce non-stoichiometric results, as shown in Fig. 2. XRD analysis would not detect the presence of an amorphous phase; however, an amorphous phase could be detected in FT-IR spectra if vibrational modes within the amorphous phase differed substantially from the crystalline phase. In this system, the FT-IR data of final mineral residues were similar to the starting materials, suggesting that amorphous materials, if present, were in small quantities (less than ca. 2%) and/or had similar vibrational modes to crystalline material as previously described by Gorman-Lewis et al. (2008b)

The Na-boltwoodite aqueous solution reaction reached steady state conditions much faster than the boltwoodite system, within 5 days from both supersaturation and undersaturation (Fig. 3). The extent of non-stoichiometric dissolution in the Na-boltwoodite systems was much greater than for the boltwoodite systems; however, U concentration in both systems was similar. This suggests that an amorphous phase formed in both Na-boltwoodite and boltwoodite systems and controls U dissolution. Similar Si concentrations were found in all Na-boltwoodite experiments which might also suggest the precipitation of an amorphous Si phase; however, saturation indices (SI) calculated by PHREEQC with a variety of databases (WATEQ4F (Ball and Nordstrom, 1991), MINTEQA2 (Allison et al., 1990), and PHREEQE (Parkhurst et al., 1980)) indicate the solutions are undersaturated with respect to amorphous silica (SI ca. -1.1 to -1.3) and silica gel (SI ca. $-.8$ to -1.3). This suggests that pure amorphous silica phase is not responsible for the similar Si concentrations in the Na-boltwoodite system but does not rule out the possibility that an amorphous uranyl silicate or sodium uranyl silicate phase formed that has a different solubility than pure amorphous silica phase. XRD analysis indicated Na-boltwoodite as the only crystalline phase present and FT-IR data of final mineral residues were similar to the starting materials. This does not rule out the possibility of an amorphous phase present as well. Previous workers found FT-IR spectra of amorphous uranyl silicate phases to be very similar to crystalline phases (see above). Previous studies measuring the solubility of Na-

boltwoodite also reported non-stoichiometric dissolution (Ilton et al., 2006; Nguyen et al., 1992). Ilton et al. (2006) varied bicarbonate concentrations in their experiments consequently enhancing uranyl carbonate aqueous complexation, and resulting in an increase in uranium relative to aqueous silica. In this work, all systems were assumed to be in equilibrium with atmospheric CO_2 , thus in general contained significantly lower total dissolved carbonate concentrations than those in Ilton et al. (2006). The maximum dissolved carbonate concentration in our experiments was approximately 1 mM while the maximum in the Ilton et al. (2006) experiments was 50 mM. The lower carbonate concentration in our experiments reduces the extent of aqueous uranyl carbonate formation relative to that in the Ilton et al. (2006) experiments, and likely explains why aqueous silica is higher than aqueous uranium for both boltwoodite and Na-boltwoodite in our experiments.

All uranophane aqueous solution reactions reached a steady-state within 10 days (Fig. 4). The initial experiment, shown in Fig. 4d, did not contain silica gel as noted above, yet exhibited similar Si concentrations to all subsequent experiments that contained silica gel. Silica concentrations in all experiments were well within the ranges reported for amorphous silica solubility (Morey et al., 1964; Walther and Helgeson, 1977). Because the silica concentration in these systems was likely buffered by amorphous silica, the U:Si ratio in solution would not necessarily correspond to stoichiometric dissolution of uranophane. Experiments from undersaturated conditions with respect to uranium resulted in Ca:U ratios of ca. 0.6–0.8, while oversaturated experiments exhibited Ca:U ratios of ca. 0.4 at pH 3 and ca. 2.5 at pH 4. XRD patterns of experimental residues indicated uranophane as the only crystalline phase present and FT-IR data of final mineral residues were similar to the starting materials.

3.4. Solubility product calculations

Solubility product (K_{sp}) calculations are based on the reaction stoichiometry shown in Table 4. K_{sp} calculations were performed using only the data points that correspond to samples that were taken from each system after it had achieved steady-state conditions. Figs. 2–4 illustrate that in most of the experiments, after an initial relatively rapid equilibration period, a solubility plateau or steady-state occurred. Elemental concentrations varied somewhat during this steady-state period, mostly due to shifts in solution pH during the course of the experiment. In effect, these migrations in pH and elemental concentrations provide additional constraints on calculated K_{sp} value because each individual solubility measurement with its own elemental concentrations and measured pH was used to calculate a K_{sp} value, and these values were averaged over all measurements at a steady-state condition. Measured U, Si, K, Ca, and Na concentrations and corresponding measured pH values for each steady state data point that we used for the calculations are compiled in the Supplemental material Tables S1–S3. All experiments were assumed to be in equilibrium with the atmospheric CO_2 thus the partial pressure of CO_2 was taken to be $10^{-3.5}$. The concentrations of U, Si,

Table 2
Results of the elemental analyses and TG study.

Sample	Cation:U / Si:U Molar ratio	Weight loss,% (first TG step/ total)	# moles water /# moles H ⁺ (from TG data)	# moles H ⁺ (from charge balance)	Final formula
Na(UO ₂)(HSiO ₄)·X(H ₂ O)	0.93 ± 0.04/ 0.93 ± 0.04	5.61 ± 0.03/ 7.31 ± 0.16	1.25 ± 0.06/ 0.72 ± 0.08	0.80	Na _{0.93} (UO ₂) (H _{0.85} SiO ₄) _{0.93} ·1.25H ₂ O
K(UO ₂)(HSiO ₄)·X(H ₂ O)	0.75 ± 0.02/ 0.86 ± 0.04	4.41 ± 0.08/ 6.52 ± 0.16	0.97 ± 0.02/ 0.88 ± 0.09	0.68	K _{0.75} (UO ₂) (H _{0.80} SiO ₄) _{0.86} ·0.97H ₂ O
Ca(UO ₂) ₂ (HSiO ₄) ₂ ·X(H ₂ O)	1.09 ± 0.01/ 0.88 ± 0.01	11.88 ± 0.82/ 13.07 ± 0.49	5.60 ± 0.34/ 0.98 ± 0.13	0.90	Ca _{1.09} (UO ₂) ₂ (H _{0.51} SiO ₄) _{1.77} ·5.60H ₂ O

Table 3
Thermodynamic functions for formation of uranyl silicates from oxides and elements.

Phase, formula	$\Delta H_{f, \text{ox}}$, kJ/mol	$\Delta H_{f, \text{el}}$, kJ/mol	$\Delta G_{f, \text{el}}$, kJ/mol	$\Delta G_{f, \text{el}}$, kJ/mol, predicted	$\Delta S_{f, \text{el}}$, J/mol·K
Soddyite 1/2(UO ₂) ₂ (SiO ₄)·2H ₂ O	-58.9 ± 2.2	-2022.7 ± 2.5	-1826.1 ± 2.1	-1818 ± 7 Clark et al. (1998)	-659.4 ± 10.9
Boltwoodite K(UO ₂)(HSiO ₄)·H ₂ O	-251.2 ± 5.9	-2766.8 ± 6.5	-2758.6 ± 3.5	-2763 ± 8 (Clark et al. (1998)	-27.5 ± 7.3
Na-boltwoodite Na(UO ₂)(HSiO ₄)·H ₂ O	-215.8 ± 6.0	-2948.8 ± 6.6	-2725.2 ± 2.6	-2984 ± 13 (Clark et al. (1998)	-352.5 ± 7.2
Uranophane 1/2Ca(UO ₂) ₂ (HSiO ₄) ₂ ·5H ₂ O	-161.1 ± 5.4	-3399.5 ± 5.8	-3099.3 ± 5.6	-3123 ± 16 Clark et al. (1998)	-1007.6 ± 12.0

and relevant cations K, Ca, or Na, the pH of each sample, and the known amount of NO₃⁻ from the electrolyte and acid additions for pH adjustments were accounted for in the ionic strength calculations for each plateau data point. We used an extended Debye–Hückel equation to calculate the activity coefficients, γ_i , for each experimental condition:

$$\log \gamma_i = \frac{-Az_i^2\sqrt{I}}{1 + aB\sqrt{I}} + bI \quad (1)$$

where I and z_i represent the ionic strength and ionic charge, respectively; A and B are constants with values of 0.5105 and 0.3285 (Helgeson et al., 1981), respectively. Values for a and b are electrolyte specific, and we used values from Helgeson et al. Although the dominant cations in solution are Na⁺, K⁺, and UO₂²⁺ and Ca²⁺ for the Na-boltwoodite, boltwoodite, and uranophane systems, respectively, we used a and b values for RbNO₃ of 5.22 and 0.062 in order to be consistent with previous uranyl mineral solubility studies (Gorman-Lewis et al., 2008a; Gorman-Lewis et al., 2007) that chose RbNO₃ as the closest approximation for solutions with UO₂²⁺ as the dominant cation. Standard states employed in this study for solid phases and for H₂O are the pure mineral or fluid, respectively, at the temperature and pressure of the experiments, and the solutions are dilute enough that we assume the activity of H₂O to be unity in all cases. The standard state for aqueous species is defined as a hypothetical one molal solution whose behavior is that of infinite dilution. Molal activity coefficients of neutral aqueous species are assumed to be unity. With these standard states, solubility product calculations for each plateau data point take into consideration the aqueous complexation reactions listed in Supplemental materials Table S4 to calculate activities under each experimental condition. Uncertainties associated with the stability constants in Table S4 (errors not shown) were not propagated through the K_{sp} calculations; however, the uncertainty

in the experimental measurements likely dominates the errors associated with the K_{sp} values and these values are reported.

Calculated solubility products, averaged for all of the plateau data points, with their 2 σ uncertainties for each phase, are listed in Table 4. Solubility product calculations for experiments in which steady state was approached from undersaturation are within experimental uncertainty of the values determined from supersaturation experiments for all experimental systems. Experiments conducted at different pH values using the same mineral phase also yield solubility product values that are within experimental uncertainty of each other. Agreement between solubility product values from under- and super-saturated experiments, and from experiments conducted at different pH values, suggests that the dissolution reactions that we modeled were formulated correctly as listed in Table 4 and that the experiments indeed reached equilibrium.

This work is the first reported solubility measurement of boltwoodite; however, two previous studies reported Na-boltwoodite solubility. Nguyen et al. (1992) performed solubility measurements from undersaturated starting conditions. Their post-experimental XRD analysis indicated the presence of additional peaks not attributed to Na-boltwoodite that appeared to correspond to soddyite peaks. Ilton et al. (2006) performed a variety of experiments measuring Na-boltwoodite dissolution; however, all of their starting conditions were from undersaturated states. Their experiments also exhibited non-stoichiometric dissolution, yet XRD analysis of the mineral residues indicated Na-boltwoodite as the only crystalline phase present. The authors were unable to identify if precipitation of an amorphous phase caused the non-stoichiometric dissolution. While these previous studies did not collect solubility data from supersaturation, our log K_{sp} value (6.07 (-0.16/+0.26)) is

Table 4
Dissolution reactions and solubility products for uranyl silicates minerals.

Mineral Phase	Dissolution reactions	Mass action equations	$\log K_{sp} \pm 2\sigma$ ($I = 0$)
Boltwoodite	$K[\text{UO}_2(\text{HSiO}_4)]\text{H}_2\text{O} + 3\text{H}^+ = \text{K}^+ + \text{UO}_2^{2+} + \text{H}_4\text{SiO}_4 + \text{H}_2\text{O}$	$K_{sp} = \frac{a_{\text{K}^+} \cdot a_{\text{UO}_2^{2+}} \cdot a_{\text{H}_4\text{SiO}_4}}{a_{\text{H}^+}^3}$	4.12 (−0.48/+0.30)
Na-boltwoodite	$\text{Na}[\text{UO}_2(\text{HSiO}_4)]\text{H}_2\text{O} + 3\text{H}^+ = \text{Na}^+ + \text{UO}_2^{2+} + \text{H}_4\text{SiO}_4 + \text{H}_2\text{O}$	$K_{sp} = \frac{a_{\text{Na}^+} \cdot a_{\text{UO}_2^{2+}} \cdot a_{\text{H}_4\text{SiO}_4}}{a_{\text{H}^+}^3}$	6.07 (−0.16/+0.26)
Uranophane	$\text{Ca}(\text{UO}_2)_2(\text{HSiO}_4)_2 \cdot 5\text{H}_2\text{O} + 6\text{H}^+ = \text{Ca}^{2+} + 2\text{UO}_2^{2+} + 2\text{H}_4\text{SiO}_4 + 5\text{H}_2\text{O}$	$K_{sp} = \frac{a_{\text{Ca}^{2+}} \cdot a_{\text{UO}_2^{2+}}^2 \cdot a_{\text{H}_4\text{SiO}_4}^2}{a_{\text{H}^+}^6}$	10.82 (−0.62/+0.29)

within error of the previous measurements by Nguyen et al. (1992) (5.82 ± 0.16) and Ilton et al. (2006) (5.86 ± 0.24 and 5.85 ± 0.26 using Pitzer and Davies equation, respectively). However, because we measured solubility from both supersaturation and undersaturation, our solubility constant value is better constrained than those from the previous studies.

The difference between our boltwoodite and Na-boltwoodite K_{sp} values indicates that the identity of interlayer cations in uranyl phases can strongly influence their solubility. Previous measurements of Na and K analogues of uranyl oxide hydrates have also exhibited similar behavior, with the Na analogue being more soluble (Gorman-Lewis et al., 2008a). Very little is known about the solid phase activity coefficients of uranyl phases; however, our work suggests even minor substitution of Na into boltwoodite could have a large impact on its solubility. This is important in environmental settings where a mixed Na–K phase would likely dominate over pure end-member phases. Nguyen et al. (1992) and Casas et al. (1994) performed solubility measurements on synthetic and natural uranophane, respectively. Synthetic uranophane experiments yielded a $\log K_{sp}$ value of 9.42 (± 0.48) while natural uranophane yielded apparent (not corrected for ionic strength effects) $\log K_{sp}$ values of 6.5 and 7.8 (± 0.8) with no report of the ionic strength of the systems. Nguyen et al. (1992) characterized their pre- and post-experimental mineral phases with XRD, confirming that no mineral alteration occurred during the course of the experiments. Post-experimental analysis on natural samples by Casas et al. (1994) consisted of scanning electron microscopy and electron dispersion spectroscopy, and these analyses revealed the presence of minerals with habits similar to rutherfordine and schoepite. Minerals other than uranophane may have controlled solution compositions in the natural uranophane experiments; consequently, K_{sp} values from Casas et al. (1994) may not reflect uranophane solubility. Our K_{sp} value is not consistent with previous measurements; however, none of the previous measurements constrained their K_{sp} values as we did with solubility measurements from both supersaturation and undersaturation experiments.

3.5. Gibbs free energy and entropy of formation

Calculated K_{sp} values for each phase can be used to obtain the standard state Gibbs free energy of formation by first calculating the standard state Gibbs free energy of reaction, ΔG_r^0 , for each dissolution reaction using the following equation:

$$\Delta G_r^0 = -2.3026 RT \bullet \log K_{sp} \quad (2)$$

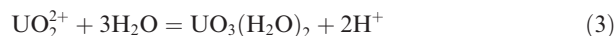
where R is the universal gas constant and T is absolute temperature. We used known standard state Gibbs free energies of formation of other components in the dissolution reactions (Table 4) and the calculated values of ΔG_r^0 to obtain the standard-state Gibbs free energies of formation of the three solid phases. Standard state Gibbs free energies of formation, obtained from Cox et al. (1989), for $\Delta G_f^0(\text{UO}_2^{2+})$, $\Delta G_f^0(\text{K}^+)$, $\Delta G_f^0(\text{Na}^+)$, $\Delta G_f^0(\text{Ca}^{2+})$, $\Delta G_f^0(\text{H}_4\text{SiO}_4)$, and $\Delta G_f^0(\text{H}_2\text{O})$ are -952.6 ± 1.7 kJ/mol, -282.5 ± 0.1 kJ/mol, -262.0 ± 0.1 kJ/mol, -1307.7 ± 1.2 kJ/mol, -552.8 ± 1.1 kJ/mol and -237.1 ± 0.1 kJ/mol, respectively. To obtain the 2σ errors associated with the ΔG_r^0 values, we propagated the largest error associated with the respective $\log K_{sp}$ values. Each data point from a solubility measurement yields calculated values for the standard state Gibbs free energy of formation for the mineral of interest, and the average value for each mineral is reported in Table 3. The 2σ errors are calculated from propagating the errors associated with the ΔG_f^0 values of the mineral phase constituents and ΔG_r^0 .

Chen et al. (1999) and Clark et al. (1998) created the database of formation enthalpies and Gibbs energies predicted for several environmentally relevant U-bearing phases. Predicted values for uranyl silicates are shown in Table 3 in comparison with the data in the current study. Predicted ΔG_f^0 for boltwoodite and uranophane are in reasonable agreement with the reported results, however the Gibbs free energy of formation for Na-boltwoodite determined from our solubility measurements is more than 200 kJ/mol more positive than the predicted value. The reasons for this discrepancy are not clear.

4. DISCUSSION

Uranyl silicate minerals are abundant on the surface of uraninite, (UO_{2+x}) exposed to groundwater (Finch and Ewing, 1992). Formation of silicates is controlled by the Si concentration in solution and direct precipitation of uranyl silicates from solution requires extremely high Si concentrations. Under lower silica saturation conditions, the initial precipitation of mixed schoepite $[(\text{UO}_2)_8\text{O}_2(\text{OH})_{12}](\text{H}_2\text{O})_{12}]$ and metaschoepite $[\text{UO}_3(\text{H}_2\text{O})_2]$ is favored. Precipitation is in turn followed by irreversible dehydration and structural rearrangement with the formation of dehydrated schoepite of approximate stoichiometry $\text{UO}_3(\text{H}_2\text{O})_{0.8}$ (Finch and Ewing, 1992; O'Hare et al., 1988). Those uranyl hydroxides are found to be the first stable alteration product of uraninite corrosion. Reaction (3), Eq. (4) and Fig. 5a indeed indicate that such formations are favorable under both natural

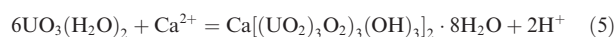
water and waste tanks conditions even if concentration of dissolved uranium is relatively low (data are taken from Gorman-Lewis et al., 2008a).



$$\Delta G_m^0 = 31.8 \pm 3.9 \text{ kJ/mol}$$

$$\Delta G_m = \Delta G_m^0 + \text{RT} \ln \left[\frac{a(\text{H}^+)^2}{a(\text{UO}_2^{2+})} \right] \quad (4)$$

Becquerelite, $\text{Ca}[(\text{UO}_2)_3\text{O}_2(\text{OH})_3]_2 \cdot 8\text{H}_2\text{O}$, has been also observed among the first alteration products of uraninite. Finch and Ewing (1992) found that becquerelite is likely to replace schoepite if additional Ca^{2+} can be supplied from groundwater. Indeed, according to reaction 5 and Eq. (6), shown in Fig. 5b, the formation of becquerelite becomes thermodynamically favorable at higher pH and in the presence of significant Ca^{2+} :

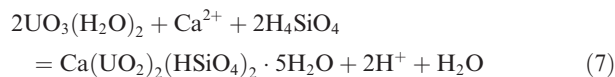


$$\Delta G_m^0 = 40.2 \pm 27.5 \text{ kJ/mol}$$

$$\Delta G_m = \Delta G_m^0 + \text{RT} \ln \left[\frac{a(\text{H}^+)^2}{a(\text{Ca}^{2+})} \right] \quad (6)$$

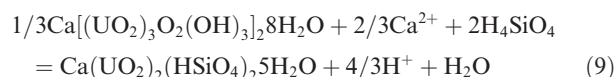
For example, under Ca^{2+} activities of 10^{-3} – 10^{-5} mol, as have been found in Yucca Mountain groundwater (Kerrisk, 1987), becquerelite is stable at pH above 5–5.5. Wogelius et al. (2007) also suggested that becquerelite easily forms as a direct product of *in situ* oxidation of UO_2 if Ca^{2+} is leached from other mineral surfaces.

Prolonged exposure of schoepite or becquerelite to groundwater enriched with both Ca^{2+} and silicate leads to complete alteration of minerals to uranyl silicates, with uranophane and soddyite being the most abundant. Reactions (7) and (9) for uranophane formation in aqueous solution have negative standard Gibbs free energies, indicating that this formation is indeed favorable under standard state conditions.



$$\Delta G_m^0 = -3.6 \pm 14.1 \text{ kJ/mol}$$

$$\Delta G_m = \Delta G_m^0 + \text{RT} \ln \left[\frac{a(\text{H}^+)^2}{a(\text{Ca}^{2+})a(\text{H}_4\text{SiO}_4)^2} \right] \quad (8)$$

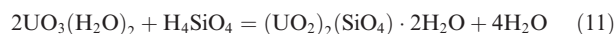


$$\Delta G_m^0 = -17.0 \pm 15.1 \text{ kJ/mol}$$

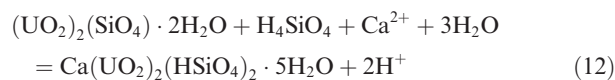
$$\Delta G_m = \Delta G_m^0 + \text{RT} \ln \left[\frac{a(\text{H}^+)^{4/3}}{a(\text{Ca}^{2+})^{2/3}a(\text{H}_4\text{SiO}_4)^2} \right] \quad (10)$$

These reactions are consistent with the observation of Wronkiewicz (Wronkiewicz et al., 1992) that formation of uranophane is usually preceded by becquerelite appearance and rarely occurs directly from schoepite. Also Finch and Ewing (1992) reported that becquerelite has been found in contact with muscovite and therefore is stable at high silica content. It often coexists with uranophane. Fig. 6(a) and (b) show the stability fields of becquerelite and uranophane at a fixed Ca^{2+} activity of 10^{-3} mol, equal to the approximate groundwater Ca^{2+} content in the Yucca Mountain area and at a silicate activity of 10^{-4} mol. Thus, the favorable conditions for forming less soluble uranophane would be higher pH at higher Ca^{2+} concentrations.

Soddyite forms even more readily from metaschoepite (reaction 11). However, the exposure of soddyite to Ca^{2+} -rich solutions does not always favor the formation of uranophane (reaction 12):



$$\Delta G_m^0 = -28.9 \pm 15.5 \text{ kJ/mol}$$



$$\Delta G_m^0 = 25.2 \pm 12.7 \text{ kJ/mol}$$

A plot of H_4SiO_4 activity vs. pH of reaction 12 at fixed 10^{-3} mol Ca^{2+} indicates that under environmental conditions uranophane would be more stable than soddyite (Fig. 7). The H_4SiO_4 activity – $\text{Ca}^{2+}/(\text{H}^+)^2$ activity diagram for the CaO – UO_3 – SiO_2 – H_2O system predicted by Chen et al. (1999) agrees with our results.

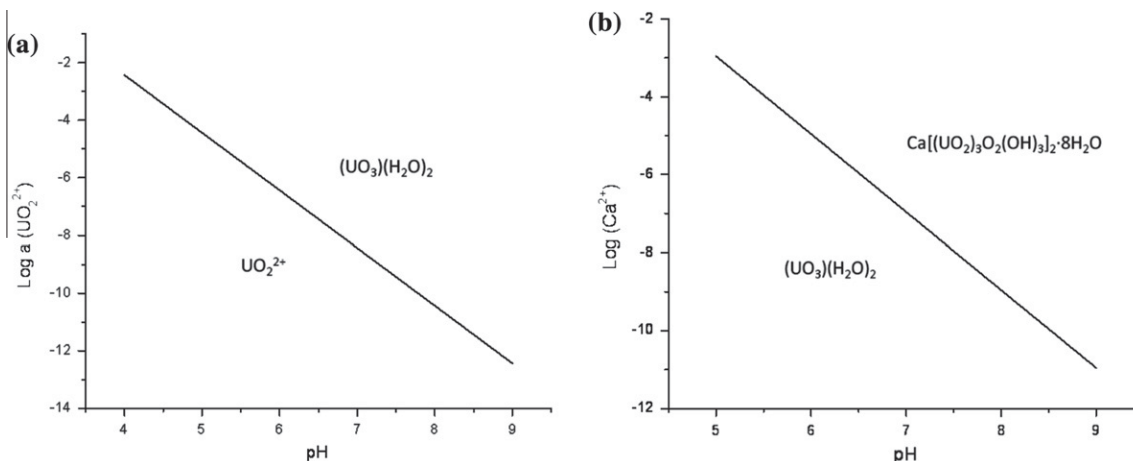


Fig. 5. pH – $\text{Log } a(\text{UO}_2^{2+})$ diagrams for the formation of metaschoepite (a) and pH – $\text{Log } a(\text{Ca}^{2+})$ diagram for becquerelite (b).

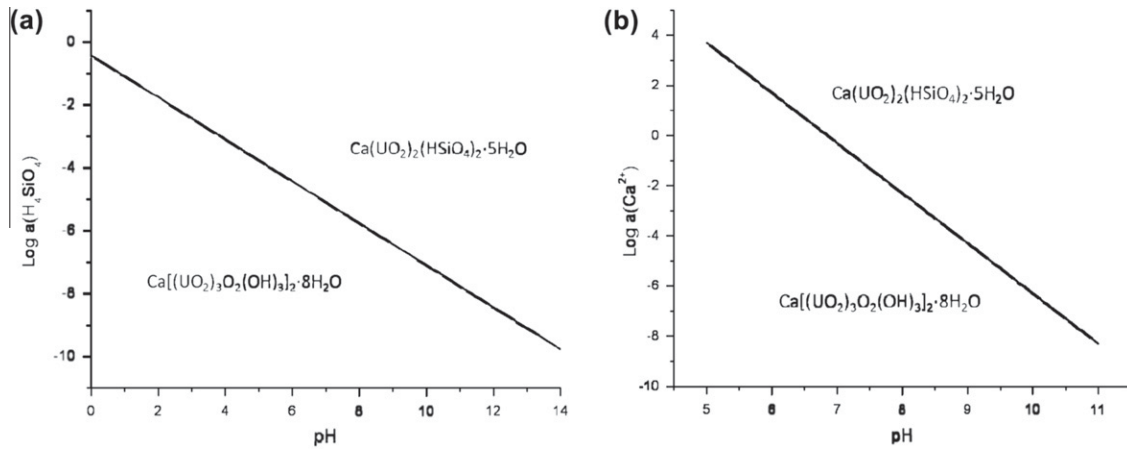


Fig. 6. The bequerelite/uranophane equilibrium at different H_4SiO_4 (a) and Ca^{2+} (b) activities as a function of pH.

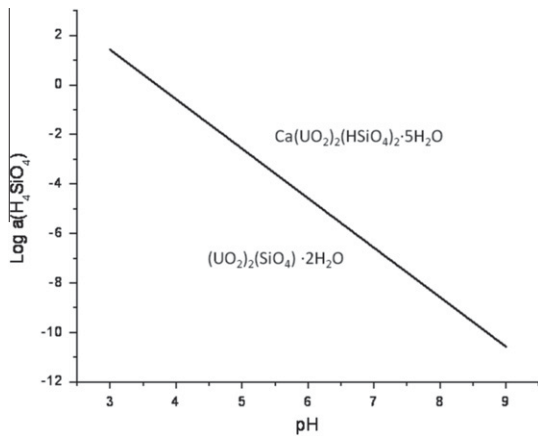
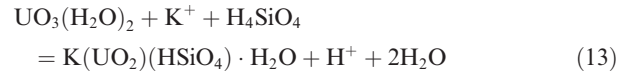


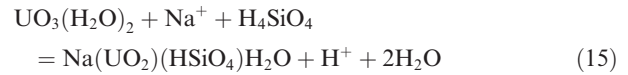
Fig. 7. pH – $\text{Log } a(\text{H}_4\text{SiO}_4)$ diagram for the system soddyite – uranophane.

In K^+ - and Na^+ -rich silica-bearing water, boltwoodite, $\text{K}(\text{UO}_2)(\text{HSiO}_4) \cdot \text{H}_2\text{O}$, and Na-boltwoodite, $\text{Na}(\text{UO}_2)(\text{HSiO}_4) \cdot \text{H}_2\text{O}$, phases can be found (Wronkiewicz et al., 1992, 1996). The formation of both minerals from metaschoepite is thermodynamically favorable under environmental conditions (shown in Fig. 8a and b, in according to reactions 14 and 16 at the fixed K^+ or Na^+ concentration 5×10^{-4}), however K-boltwoodite can form under more acidic pH.



$$\Delta G_m^0 = -10.7 \pm 8.4 \text{ kJ/mol}$$

$$\Delta G_m = \Delta G_m^0 + RT \ln[a(\text{H}^+)/a(\text{H}_4\text{SiO}_4)] \quad (14)$$



$$\Delta G_m^0 = 2.2 \pm 8.1 \text{ kJ/mol}$$

$$\Delta G_m = \Delta G_m^0 + RT \ln[a(\text{H}^+)/a(\text{Na}^+)a(\text{H}_4\text{SiO}_4)] \quad (16)$$

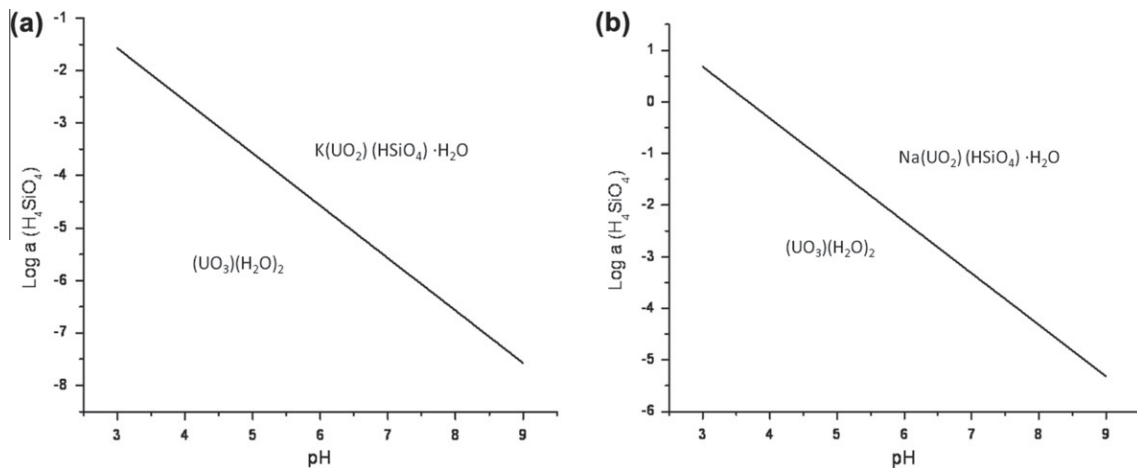
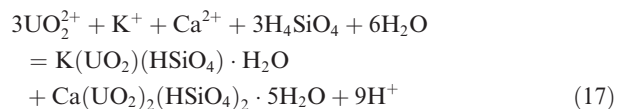


Fig. 8. pH – $\text{Log } a(\text{H}_4\text{SiO}_4)$ equilibrium diagrams at fixed K^+ and Na^+ concentration 5×10^{-4} mol for the boltwoodite (a) and Na-boltwoodite (b) formation from metaschoepite, respectively.

Uranophane and boltwoodite are also found to be dominant phases in contaminated sediments close to leaking tank farms at the Hanford Site (Um et al., 2009). Their formation reaction can be expressed as follows:



$$\Delta G_m^0 = 81.0 \pm 16.1 \text{ kJ/mol}$$

$$\Delta G_m = \Delta G_m^0 + \text{RTln}([\text{H}^+]^9/[\text{Ca}^{2+}][\text{H}_4\text{SiO}_4]^3[\text{K}^+][\text{UO}_2^{2+}]^3) \quad (18)$$

According to reaction 17 and Eq. (18), at a typical reported composition of leaking Hanford tank waste (UO_2^{2+} activity of 10^{-4} , Ca^{2+} activity of 3.5×10^{-3} , K^+ of 2.5×10^{-2} , and H_4SiO_4 activity of 4.5×10^{-3} (Um et al., 2009), our thermodynamic data confirm that these minerals are thermodynamically stable at any pH above 4, a result which is consistent with groundwater compositions and observations at the Hanford Site (Um et al., 2009).

ACKNOWLEDGEMENTS

This material is based upon work supported as part of the Materials Science of Actinides, an Energy Frontier Research Center funded by the U.S. Department of Energy, Office of Science, Office of Basic Energy Sciences under Award Number DE-SC0001089. Funding for the beginning stages of this project (prior to EFRC) was provided by a U.S. Department of Energy, Office of Science and Technology and International (OST&I) grant under the Source Term Thrust program.

APPENDIX A. SUPPLEMENTARY DATA

Supplementary data associated with this article can be found, in the online version, at doi:10.1016/j.gca.2011.06.041.

REFERENCES

- Allison J. D., Brown D. S. and Novo-Gradac K. J. (1990) *MINTEQA2/PRODEFA2 – A geochemical assessment model for environmental systems – version 3.0 user's manual: Environmental Research Laboratory, Office of Research and Development, U.S. Environmental Protection Agency, Athens, Georgia*, 106 p.
- Arnold P. L., Potter N. A., Magnani N., Apostolidis C., Griveau J. C., Colineau E., Morgenstern A., Caciuffo R. and Love J. B. (2010) Synthesis of bimetallic uranium and neptunium complexes of a binucleating macrocycle and determination of the solid-state structure by magnetic analysis. *Inorg. Chem.* **49**, 5341–5343.
- Ball, J.W. and Nordstrom, D. K. (1991) User's manual for WATEQ4F, with revised thermodynamic database and test cases for calculating speciation of major, trace, and redox elements in natural waters. Menlo Park: U.S. Geological Survey Open-File Report. 91-193.
- Barger J. R., Bernier-Latmani R., Giammar D. E. and Tebo B. M. (2008) Biogenic uraninite nanoparticles and their importance for uranium remediation. *Elements* **4**, 407–412.
- Burns P. C. (1998) The structure of boltwoodite and implications of solid solution toward sodium boltwoodite. *Can. Mineral.* **36**, 1069–1075.
- Burns P. C. (2005) U^{6+} minerals and inorganic compounds: insights into an expanded structural hierarchy of crystal structures. *Can. Mineral.* **43**, 1839–1894.
- Bruno J., Casas I., Finch R. J., Cera E. and Ewing R. C. (1994) Kinetic and thermodynamic studies of uranium minerals. Assessment of the long-term evolution of spent nuclear fuel. *SKB Tech. Rep.* **94**, 73.
- Catalano J. G., Heald S. M., Zachara J. M. and Brown G. E. (2004) Spectroscopic and Diffraction Study of Uranium Speciation in Contaminated Vadose Zone Sediments from the Hanford Site, Washington State. *Environ. Sci. Technol.* **38**, 2822–2828.
- Cejka J. (1999) Infrared spectroscopy and thermal analysis of the uranyl minerals. *Rev. Mineral.* **38**, 521–622.
- Chen F., Ewing R. C. and Clark S. B. (1999) The Gibbs free energies and enthalpies of formation of U^{6+} phases: an empirical method of prediction. *Am. Mineral.* **84**, 650–664.
- Clark S. B., Ewing R. C. and Schaumloffel J. C. (1998) A method to predict free energies of formation of mineral phases in the U(VI)- SiO_2 - H_2O system. *J. Alloys Compd.* **271**, 189–193.
- Cox J. D., Wagman D. D., and Medvedev V. A. (1989) *CODATA Key Values for Thermodynamics*. pp. 271
- Deditius A. P., Utsunomiya S. and Ewing R. C. (2007) Alteration of coffinite (USiO_4) under reducing and oxidizing conditions. *Mater. Res. Soc. Symp. Proc.* **985**, 47–52.
- Demartin F., Gramaccioli C. M., Pilati T. (1992) The importance of accurate crystal structure determination of uranium minerals. II. Soddyite $(\text{UO}_2)_2(\text{SiO}_4) \cdot 2\text{H}_2\text{O}$. *Acta Crystallogr.*, C(48), 1-4.
- Finch R. J. and Ewing R. C. (1992) The Corrosion of Uraninite under Oxidizing Conditions. *J. Nucl. Mater.* **190**, 133–156.
- Finch R. J. and Hawthorne F. C. (1998) Structural relations among schoepite, metaschoepite and dehydrated schoepite. *Can. Mineral.* **36**, 831–845.
- Gorman-Lewis D., Mazeina L., Fein J. B., Szymanowski J. E. S., Burns P. C. and Navrotsky A. (2007) Thermodynamic properties of soddyite from solubility and calorimetry measurements. *J. Chem. Thermodyn.* **39**, 568–575.
- Gorman-Lewis D., Fein J. B., Burns P. C., Szymanowski J. E. S. and Converse J. (2008a) Solubility measurements of the uranyl oxide hydrate phases metaschoepite, compreignacite, Na-compreignacite, becquerelite, and clarkeite. *J. Chem. Thermodyn.* **40**, 980–990.
- Gorman-Lewis D., Skanthakumar S., Jensen M. P., Mekki S., Nagy K. L. and Soderholm L. (2008b) FTIR characterization of amorphous uranyl-silicates. *Chem. Geol.* **253**, 136–140.
- Gorman-Lewis D., Shvareva T. Y., Kubatko K.-A., Burns P. C., Wellman D. M., McNamara B., Szymanowski J. E. S., Navrotsky A. and Fein J. B. (2009) Thermodynamic properties of autunite, uranyl hydrogen phosphate, and uranyl orthophosphate from solubility and calorimetric measurements. *Environ. Sci. Technol.* **43**, 7416–7422.
- Helean K. B., Navrotsky A., Vance E. R., Carter M. L., Ebbinghaus B., Krikorian O., Lian J., Wang L. M. and Catalano J. G. (2002) Enthalpies of formation of Ce-pyrochlore, $\text{Ca}_{0.93}\text{Ce}_{1.00}\text{Ti}_{2.035}\text{O}_{7.00}$, U-pyrochlore, $\text{Ca}_{1.46}\text{U}_{0.23}^{4+}\text{U}_{0.46}^{6+}\text{Ti}_{1.85}\text{O}_{7.00}$ and Gd-pyrochlore, $\text{Gd}_2\text{Ti}_2\text{O}_7$: three materials relevant to the proposed waste form for excess weapons plutonium. *J. Nucl. Mater.* **303**, 226–239.
- Helgeson H. C., Kirkham D. H. and Flowers G. C. (1981) Theoretical prediction of the thermodynamic behavior of aqueous-electrolytes at high-pressures and temperatures: iv. calculation of activity-coefficients, osmotic coefficients, and apparent molal and standard and relative partial molal properties to 600 C and 5 KB. *Am. J. Science* **281**, 1249–1516.

- Illingworth J. A. (1981) A Common Source of Error in pH Measurements. *Biochem. J.* **195**, 259–262.
- Ilton E. S., Liu C., Yantasee W., Wang Z., Moore D. A., Felmy A. R. and Zachara J. M. (2006) The dissolution of synthetic Nabboltwoodite in sodium carbonate solutions. *Geochim. Cosmochim. Acta* **70**, 4836–4849.
- Kerrisk J. F. (1987) Groundwater chemistry at Yucca Mountain, Nevada, and vicinity, Los Alamos Natl. Lab Report, Los Alamos, NM, USA. pp. 124.
- Kubatko K.-A., Helean K., Navrotsky A. and Burns P. C. (2005) Thermodynamics of uranyl minerals: Enthalpies of formation of rutherfordine, UO_2CO_3 , andersonite, $\text{Na}_2\text{CaUO}_2(\text{CO}_3)_3(\text{H}_2\text{O})_5$, and grimselite, $\text{K}_3\text{NaUO}_2(\text{CO}_3)_3\text{H}_2\text{O}$. *Am. Mineral.* **90**, 1284–1290.
- Kubatko K.-A., Helean K., Navrotsky A. and Burns P. C. (2006) Thermodynamics of uranyl minerals: enthalpies of formation of uranyl oxide hydrates. *Am. Mineral.* **91**, 658–666.
- Langmuir D. (1978) Uranium solution-mineral equilibria at low temperatures with applications to sedimentary ore deposits. *Geochim. Cosmochim. Acta* **42**, 547–569.
- Le S.-N. and Navrotsky A. (2007) Energetics of phosphate frameworks containing zinc and cobalt: NaZnPO_4 , $\text{NaH}(\text{ZnPO}_4)_2$, $\text{NaZnPO}_4 \cdot \text{H}_2\text{O}$, $\text{NaZnPO}_4 \cdot 4/3\text{H}_2\text{O}$, and $\text{NaCo}_{1-x}\text{Zn}_x\text{PO}_4 \cdot 4/3\text{H}_2\text{O}$. *J. Solid State Chem.* **180**, 2443–2451.
- Le S.-N. and Navrotsky A. (2008) “Energetics of formation of alkali and ammonium cobalt and zinc phosphate frameworks. *J. Solid State Chem.* **181**, 20–29.
- Morey G. W., Fournier R. O. and Rowe J. J. (1964) The solubility of amorphous silica at 25 °C. *J. Geophys. Res.* **69**, 1995–2002.
- Navrotsky A. (1977) Progress and new directions in high-temperature calorimetry. *Phys. Chem. Minerals* **2**, 89–104.
- Navrotsky A. (1997) Progress and new directions in high temperature calorimetry revisited. *Phys. Chem. Min.* **24**, 222–241.
- Nguyen S. N., Silva R. J., Weed H. C. and Andrews J. E. (1992) Standard Gibbs free-energies of formation at the temperature 303.15 K of four uranyl silicates – soddyite, uranophane, sodium boltwoodite, and sodium weeksite. *J. Chem. Thermodyn.* **24**, 359–376.
- Nitsche H. (1997) Actinides in the environment. *Proc. Robert A. Welch Found. Conf. Chem. Res.* **41**, 127–164.
- O’Hare P. A. G., Lewis B. M. and Nguyen S. N. (1988) Thermochemistry of uranium compounds. XVII. Standard molar enthalpy of formation at 298.15 K of dehydrated schoepite (uranium oxide hydrate ($\text{UO}_3 \cdot 0.9\text{H}_2\text{O}$)). Thermodynamics of (schoepite + dehydrated schoepite + water). *J. Chem. Thermodyn.* **20**, 1287–1296.
- Parkhurst, D.L., Thorstenson, D.C., and Plummer, L.N., (1980) PHREEQE—A computer program for geochemical calculations: U.S. Geological Survey Water-Resources Investigations Report 80-96, pp. 195 (Revised and reprinted August, 1990).
- Pearcy E. C., Prikryl J. D., Murphy W. M. and Leslie B. W. (1994) Alteration of uraninite from the Nopal I deposit, Pena Blanca District, Chihuahua, Mexico Compared to degradation of spent nuclear fuel in the proposed U.S. high-level nuclear waste repository at Yucca Mountain, Nevada. *Appl. Geochem.* **9**, 713–732.
- Robie R. A., and Hemingway B. S. (1995) Thermodynamic properties of minerals and related substances at 298.15 K and 1 bar pressure and at higher temperatures. U.S. Geological Survey Bulletin 2131, 461.
- Smith D. W. (1987) An acidity scale for binary oxides. *J. Chem. Educ.* **64**, 480–481.
- Tessier F. and Navrotsky A. (2000) Thermochemistry of phosphorus oxynitrides: PON and LiNaPON glasses. *Chem. Mater.* **12**, 148–154.
- Um W., Wang Z., Serne R. J., Williams B. D., Brown C. F., Dodge C. J. and Francis A. J. (2009) Uranium Phases in Contaminated Sediments below Hanford’s U Tank Farm. *Environ. Sci. Technol.* **43**, 4280–4286.
- Urbanec Z., Mrazek Z. and Cejka J. (1985) Thermal and infrared spectrum analyses of some uranyl silicate minerals. *Thermochim. Acta* **93**, 525–528.
- Ushakov S. V., Cheng J., Navrotsky A., Wu J. R. and Haile S. M. (2002) Formation enthalpies of tetravalent lanthanide perovskites by high temperature oxide melt solution calorimetry. *Mater. Res. Soc. Symp. Proc.* **718**, 71–76.
- Ushakov S. V., Navrotsky A., Farmer J. M. and Boatner L. A. (2004) Thermochemistry of the alkali rare-earth double phosphates, $\text{A}_3\text{Re}(\text{PO}_4)_2$. *J. Mater. Res.* **19**, 2165–2175.
- Walther J. V. and Helgeson H. C. (1977) Calculation of the thermodynamic properties of aqueous silica and the solubility of quartz and its polymorphs at high pressures and temperatures. *Am. J. Sci.* **277**, 1315–1351.
- Wogelius R. A., Morris P. M., Kertesz M. A., Chardon E., Stark A. I. R., Warren M. and Brydie J. R. (2007) Mineral surface reactivity and mass transfer in environmental mineralogy. *Eur. J. Mineral.* **19**, 297–307.
- Wronkiewicz D. J., Bates J. K., Gerding T. J., Veleckis E. and Tani B. S. (1992) Uranium release and secondary phase formation during unsaturated testing of uranium dioxide at 90 °C. *J. Nucl. Mater.* **190**, 107–127.
- Wronkiewicz D. J., Bates J. K., Wolf S. F. and Buck E. C. (1996) Ten-year results from unsaturated drip tests with UO_2 at 90 °C: implications for the corrosion of spent nuclear fuel. *J. Nucl. Mater.* **238**, 78–95.

Associate editor: George R. Helz